SAE International

2012-01-1166
Published 04/16/2012

doi:10.4271/2012-01-1166
saepcmech.saejournals.org

The Aerodynamic Characteristics of a Fully Deformable Formula One Wind Tunnel Tyre

A. J. Sprot, D. B. Sims-Williams and R. G. Dominy
Durham University

ABSTRACT

Competitive aerodynamic performance of a Formula One car relies upon total understanding of the downstream wake of exposed rotating wheels. Sensitivities to the downstream vortices and low stagnation-pressure regions lead to subtle design decisions in bargeboards, side-pods and the leading edge of the highly sensitive floor region. A significant proportion of an F1 aerodynamicist's time is spent dealing with front wheel wake structures and indeed much of the front wing is developed to provide pressure gradients and vortex structures to control this wake.

Wind tunnel testing of scaled deformable tyres has become a common occurrence in F1 in recent years although there is a significant lack of available literature, academic or otherwise. Due to high vertical loads experienced by a grand prix car and the relatively high levels of camber used for mechanical advantage, the use of a rigid tyre is no longer considered suitable for the accurate simulation of an F1 wheel wake. This investigation has studied in detail the aerodynamic consequences born from sidewall bulge and contact patch parameters through the use of an innovative rotating sidewall scanning technique, static contact patch measurements, five-hole pressure-probe wake measurements, Particle Image Velocimetry (PIV) and load-cell drag measurements. A table of three-dimensional coordinates for the maximum and minimum deformation levels has been included in this paper to enable further CFD studies to be undertaken.

For longevity of tyre and moving ground plane, deformation levels are often fairly conservative in industrial and race team applications. The work presented here includes a full range of on-track axle heights, which far exceed those usually tested in the aforementioned settings and the aerodynamic consequences of under-deforming have been identified. It has been concluded that insufficient deformation of the tyre sidewalls leads to a significant overestimate in the width of the wake as well as the aerodynamic loads associated with it. As a result of this study, the most sensitive parameters of a deformable tyre relating to aerodynamic testing have been identified and summarised. For development of an F1 car, a compromise in tyre pressure is considered less detrimental to the downstream wake compared to providing insufficient deformation with an incorrect axle height.

CITATION: Sprot, A., Sims-Williams, D. and Dominy, R., "The Aerodynamic Characteristics of a Fully Deformable Formula One Wind Tunnel Tyre," *SAE Int. J. Passeng. Cars - Mech. Syst.* 5(2):2012, doi:10.4271/2012-01-1166.

INTRODUCTION

The aerodynamic performance of a Formula One (F1) car depends heavily upon a highly complex system of pressure gradients and vortex structures in order to generate negative lift, known more commonly as downforce. This highly sensitive combination of features must be controllable in order to develop further and as such, they require precise understanding. As well as downforce considerations, the aerodynamic drag of an F1 car is an important feature. F1 cars often run extremely high levels of drag due to the highly aggressive aerodynamic devices on the car. In addition, it has been reported that the exposed rotating wheels of a grand prix car contribute between thirty-five and fifty percent of the overall drag of the vehicle (Dominy [1]). Whilst it may appear that downforce is more significant than drag, reducing the drag has a practical application in F1 car design. By reducing the drag of components, which do not produce useful vertical load, such as the wheels, devices such as the rear wing can become even more aggressive in order to produce more downforce for the same target drag penalty.

Aside from the forces at work, the flow structures of an F1 front wheel assembly are extremely complex. Fackrell and Harvey [2,3] and in more detail in Fackrell [4], performed the first significant comprehensive aerodynamic study of an exposed race car wheel in isolation. Their work showed the characteristic positive lift generated by a wheel and also showed that when rotating, both the lift and drag of the wheel are reduced due to the forward movement of the upper

separation point. Because of this sensitivity, it is clear that the wheels of a grand prix car have significant contributions to the overall aerodynamic performance of the car.

A significant proportion of the downforce of an F1 car is produced under the large flat floor in close proximity to the ground. Regulations of the sport, which are also responsible for the exposed wheel nature of the formula, heavily restrict the size and location of the floor. The leading edge, in particular, is an area in which a large proportion of downforce is developed and this propagates down to the rear of the car where the expansion from the diffuser encourages further load. Because the leading edge of the floor is in close proximity to the downstream wake of the front wheel assembly, its performance can be enhanced or hindered by subtle changes to the front wheel wake.

Measuring the lift of a rotating wheel is a complex and contentious procedure. It is not considered reliable due to the varying reaction force with the ground as separating the mechanical and aerodynamic forces of any experiment becomes problematic in this situation. Morelli [5] attempted to overcome this by breaking the contact of the wheel with the floor. In doing so, the results of his experiments showed significant changes to the flow-field. The force measurements showed negative lift from a rotating wheel. This was explained due to the gap under the wheel causing acceleration and therefore low pressure pulling the wheel down. Stapleford and Carr [6] performed the same experiment with a sealed gap using strips of paper with much more conventional positive lift and drag results.

Saddlington et al. [7] combined published work of the flow-field combined with their own LDA measurements to produce a comprehensive description of the downstream flow-field. Their description comprises two large counter-rotating vortices generated by large central downwash and two upper counter-rotating vortices generated from the tyre's shoulder. Knowles' conclusion from this work was that the sidewall of the tyre formed these features. Fackrell and Harvey's work, as above [2], showed the sidewall profile as well as the aspect ratio have significant effects on the aerodynamic characteristics of the wheel.

Mears et al. [8, 9, 10] showed the forces at work on a rotating wheel by using a radio telemetry system. By measuring the static pressure distribution at several points on the tread in different rotational positions, they confirmed the previous studies of exposed wheel aerodynamics as well as showing experimental proof of Fackrell's 'jetting' phenomenon. Jetting is the process of air being squeezed out of the frontal contact patch and is responsible for an area of low pressure around the contact patch. This effect is sometimes referred to as 'tyre squirt' and can be a detrimental contribution to the delicate F1 aerodynamic system. More detail on this can be found in Mears [11].

Sprot et al. [12] showed for a front wheel assembly including brake cooling ducts, higher levels of through-hub flow were of a significant drag benefit due to preventing the dominant low hub-flow related spillage drag. This also had the benefit of moving the dominant counter-rotating vortices toward the outboard of the car. This prevents the inboard feature impacting upon the sensitive floor area as well as the sidepods and cooling ducts. The counter-rotating features downstream of the wheel can also assist the floor pressure distribution. Under normal circumstances, the low pressure under the floor results in an inwash from the low quality (low stagnation pressure) air in the tyre's wake. This is not good for diffuser performance and also means that this particular mass-flow is only acting on part of the floor. By sealing the outside of the floor, or providing outwash at the floor level, this encourages much higher energy flow to enter from the front of the floor and therefore act upon the whole surface of the floor, giving more load and more diffuser potential. The inboard vortex of an isolated wheel, as described by Saddlington et al. [7] would provide the opposite, detrimental inwash. Moving the whole structure outboard or disturbing the inboard feature entirely, whilst minimising stagnation pressure losses is something aerodynamicists strive to achieve.

F1 tyres have characteristically high sidewalls. Due to this, it is often the case that these are considered as part of the suspension geometry. Because of vortex features, the jetting phenomenon, through-hub flow and wake-breathing, the shape of the tyre is significant to its aerodynamic performance. As an F1 car drives at varying speeds, it generates varying levels of downforce. For example, higher speed corners will provide more compression of the suspension springs and the sidewall whereas lower speed corners will provide relatively little deflection. There is also the question of steering angle and slip in the system. Due to these parameters, the sidewall and contact patch of a tyre changes significantly many times per lap. This provides another element of unpredictability to the already complicated flow structure.

Traditionally, scale wind tunnel tests are performed with rigid tyres with a fixed sidewall shape. Only three known studies are reported to include an element of deformation in race car wheels. These were by Purvis [13], Axerio et al. [14] and Mears [11], as above. However, the latter case used a pneumatic tyre but it was treated as rigid with a high inflation pressure and negligible vertical load. Pneumatic tyres are also used in full scale testing but there is a significant lack of published work on the characteristics of setup parameters such as vertical load or tyre pressure. The advantages of using a deformable tyre include the ability to have a full and consistent contact patch as opposed to contact line, hence more suitable to a real world simulation. A tyre under load also creates a sidewall bulge and the effect of camber can be effectively modelled without making the wheel conical. Purvis' wheel only considered the former point by having a tread made from deformable foam. Despite this, an important conclusion was achieved which showed that the width of the wake changes linearly with the width of the contact patch. Therefore it is more desirable to perform flow-field studies

on a fully deformable tyre as intricacies can be identified which would be otherwise overlooked.

The work of Axerio et al. comprised a comparison of Particle Image Velocimetry (PIV) techniques against two Computational Fluid Dynamics (CFD) methodologies. This work concluded by illustrating how the wake structure of the wheel, particularly the vortex centres of the two lower lobes, oscillate in time. To this date, there has not been a reported study describing the subtleties of deformable tyre flow structures. In order to use these as a tool for aerodynamic development, their performance and characteristics should be fully understood in isolation.

EXPERIMENTAL CONFIGURATION AND TECHNIQUES

WIND TUNNEL CONFIGURATION

The Durham University $2m^2$ open-jet open-return wind tunnel (as reported by Sims-Williams et al. [15, 16]) was used in this investigation. The wheel model being used generated an average jet blockage (average due to the deformable nature of the tyre changing the projected frontal area) of 3.4% including the sting arm and brake scoop and the tests were performed at a Reynolds number (based upon wheel diameter) of $Re = 4.80\times10^5$ (in the supercritical regime, the importance of operating in this region was emphasised by Fackrell [4]). The tests were performed with a moving ground plane synchronised with the free stream. These configurations are consistent with accepted values for accurate wind tunnel testing of a rotating, exposed wheel.

THE DEFORMABLE TYRE

A fully deformable pneumatic tyre designed specifically for wind tunnel operation was used in this experiment. The tyre was typical of those used by the teams for wind tunnel testing during a recent F1 season. It was 50% scale with an aspect ratio of 0.53 (based on tyre diameter and maximum width) compliant with the current regulations of the sport. The sidewall construction had been carefully designed by the manufacturer in order to match the exact deformations seen on-track under varying loads.

There are many parameters that can be used to set deformation on a pneumatic tyre. Vertical load, tyre pressure and axle height are all valid variables. In this case, axle height was used as the primary control variable as this was considered the most repeatable condition. A set of axle heights was chosen to match F1 cars under straight-line conditions over a range of speeds from slow corner exits up to end-of-straight conditions. These can be seen in Table 1. Essentially the axle heights correspond to a linear deflection with force due to the spring approximation of the tyre sidewall combined with the velocity-squared characteristic of downforce.

Table 1. Axle height conditions used to simulate varying deformation levels.

Vehicle Speed (kph)	Mid-Rim Axle Height (mm – Model Scale)
80	159.0
120	158.0
180	155.9
250	153.3
310	150.0

The axle heights in Table 1 were set using a Baumer laser distance sensor placed on the support sting as a reference. Before testing could begin, particularly for PIV measurements, the tyre had to be balanced to a high precision. This was achieved by utilising the inbuilt load-cell normally used for drag measurements. By synchronising an optical sensor to provide a datum point with the force trace from the load-cell it was possible to see where the mass offset was on the tyre and hence where mass could be added to balance the wheel. This allowed, among other benefits, for perfectly stable PIV images to be taken while an inadequately balanced wheel would produce wheel geometry movements between image pairs that would corrupt near-wheel measurements.

APPLICATION OF DEFORMATION

The tyre required some form of vertical load in order to deflect and deform to the correct contact patch shape. It is very difficult to apply a large vertical force in a wind tunnel environment without damaging either the tyre or the belt for the moving ground plane. This usually results in a compromise in tyre pressure and axle height in order to minimise the vertical force. It could be argued that, if the tyre axle height and pressure are incorrect then an incorrect tyre profile and contact patch are being simulated which could be as bad as not simulating deformation at all. The philosophy of this experiment was to test beyond these usual compromises to obtain a detailed relationship between vertical load, tyre pressure and aerodynamic performance. Three tyre pressures were tested for this investigation. These were 0.5psi (3.4kPa), 2.0psi (13.8kPa) and 3.0psi (20.7kPa).

Deformation was applied by setting the tyre inflation pressure and axle height through the use of a ‘wheels off’ sting mounted to the inboard side of the wheel. This was extended beyond its pivot point and placed on the tip of a pneumatic cylinder mounted to the floor of the tunnel. See Figure 1 for the experimental layout. Table 2 shows the range of conditions tested and also displays the axle rise due to the centripetal reaction force caused through wheel rotation. The latter was taken into account when the wheel height was defined, as the axle height would change by up to 3.3mm depending on the level of vertical load. The measured air pressure at the pneumatic cylinder determined the vertical load. These values are therefore a maximum theoretical load

value and are intended as a reference to relative forces required for differing levels of deformation. Typically, F1 wind tunnel tests of deformable tyres do not exceed the order of 50-100N by using the rim's weight alone as the method of applying vertical load. As the table shows, this only approaches the slow-medium cornering speed conditions outlined in Table 1.

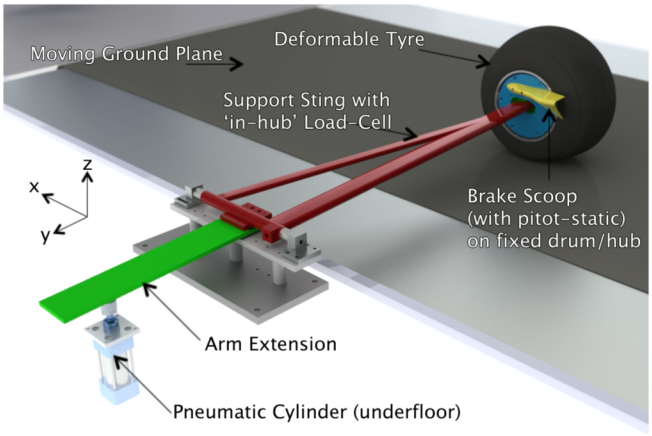

Figure 1. The experimental layout of the deformation rig in the wind tunnel.

Table 2. Vertical loads applied to meet the 50% scale axle height conditions (including centripetal axle rise).

Tyre Pressure [psi,(kPa)]	Rotating Height (mm)	Nominal Vertical Load (N)	Rotational Axle Rise (mm)
0.5, (3.4)	159	46	2.8
	156	127	2.1
	153	191	3.3
	150	240	2.9
2.0, (13.8)	159	127	1.6
	155	191	1.5
	153	240	2.0
	150	280	2.0
3.0, (20.7)	159	175	1.7
	155	240	1.8
	153	289	1.8
	150	334	2.6

The wheel was run at a typical on-track camber angle of between 3.20° and 3.45° depending on deformation levels. This is known to be a significant change from a mechanical perspective but since there is no published work on the aerodynamic effect of camber on a wheel using a deformable tyre, the significance of this cannot be quantified. The most likely significance of changing camber angles will be due to the reduction in contact patch size, emphasising inboard tread contact. This will allow air to pass underneath the tread on the outboard side for low levels of deformation (slow-speed corners) generating a similar effect to that measured by Morelli [5]. In terms of geometry changes, the deformation level and axle height will dominate this so it can be assumed that this small change in camber angle is negligible for this study.

CONTACT PATCH MEASUREMENTS

The size and shape of the contact patch of a rotating tyre are both very difficult measurements to take. As already presented, the sidewall of the tyre stretches and straightens as the wheel rotates leading to an axle height rise. This effect causes a change in sidewall shape that in turn creates a change in contact patch size. For this experiment, static measurements of the contact patch were made with axle heights set to match those of the rotating condition. By placing a transferrable ink cross on the tread of the tyre and then placing it on a piece of paper before applying the deformation, an imprint of the contact patch length and width was measured. This method did not achieve the exact contact patch shape (which is non-rectangular and assumed elliptical for area calculations) but did give useful information relating to the proportion of the tyre's width which is sealed and that which allows low-pressure air to pass underneath.

SIDEWALL PROFILE MEASUREMENTS

As the focus of this paper is on the behaviour and performance of a deformable tyre, a significant proportion of the research effort was on measuring quantitatively the subtleties of the sidewall profiles. A Baumer laser sensor was used in this process. It was calibrated against a highly reflective surface at varying distances over its 30-130mm range. The calibration was then checked with the dull matt black curved surface of the sidewall of the tyre when stationary. It was found that the average delta of the sensor on the angled and curved matt black surface relative to the highly reflective perpendicular surface was 0.8mm. This was on top of the inherent 0.3mm laser repeatability from the reflective surface test. The above delta was taken for a static section of the sidewall and due to the characteristic hysteresis of a deformable tyre, this delta is smaller than typical circumferential changes in the shape of the tyre as it rotates.

In order for the tyre to be measured in a controlled manner whilst rotating, the three-axis wind tunnel probe traverse system was used. By mounting the laser distance sensor to the end of the sting, which normally holds a five-hole pressure-probe, the laser could be traversed around the tyre in order to measure the profile. Figure 2 shows the details of this setup. In order to eliminate vibrations and other discrepancies in the measurement technique, a second laser was placed on the same mount, which measured a flat plate mounted firmly to the inboard side of the hub. This reference was subtracted from the first laser measurement in order to account for any movements of the whole wheel assembly relative to the measurement tip.

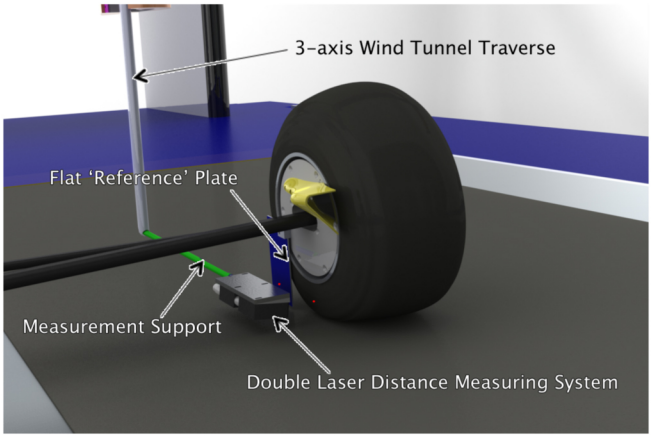

Figure 2. The sidewall profile measurement technique utilising two laser distance sensors and the wind tunnel three-axis traverse.

5-HOLE PRESSURE-PROBE MEASUREMENTS

As well as traversing a laser distance-measuring device around the wheel, the wind tunnel's three-axis traverse system was used for pressure-probe measurements in the downstream wake. Based upon an average wheel diameter of 0.32m, the planes measured were 0.5D, 1.0D, 1.5D and 2.0D from the axle in the crossplane orientation (y-z plane). The probe used was one of Durham University's in-house designed five-hole probes manufactured with a rapid prototyping machine. The probe was independently calibrated at velocities typically observed in the downstream wake of a tyre. The angular resolution of the probe was ±50° in both pitch and yaw. Although the probe is capable of measuring turbulence levels, it was used as a steady-state probe to obtain the average flow-field for comparison with other test conditions.

PARTICLE IMAGE VELOCIMETRY (PIV)

In order to measure the subtler flow physics such as recirculation and in order to interrogate regions that would be out of range for the above probe, PIV was used. A 120mJ dual head pulsed Nd:YAG system with twin high-resolution Sensicam cameras was used. Figure 3 shows the layout in detail. The laser beam was delivered to the test section via an articulated arm and was placed in the flow far downstream of the model (2.5m from the furthest rear part of the model). A longitudinal orientation was applied (x-z plane) in order to view the regions of the flow related to jetting and upper surface separation. Only the valid vectors from the two hundred image pairs per configuration were averaged to produce the vector fields presented in this paper.

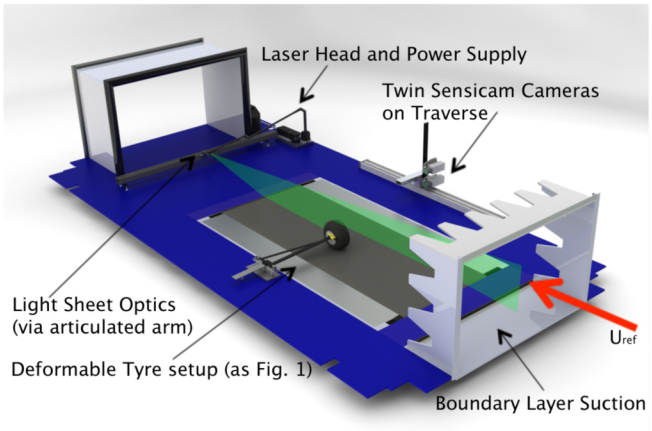

Figure 3. The PIV experimental layout.

The two cameras were placed one above the other and both synchronised to allow a 340mm total image height (1.1D) to be achieved. They were traversed downstream to allow multiple positions to be stitched together in order to provide the overall field. Each pulse was separated by 20μs which allowed a good separation of particles between images but short enough to prevent signal drop-out between image pairs. The flow was seeded using DEHS oil distributed via a compressed air fed ILATEC 40 nozzle seeder, which produces particle sizes of the order of 1μm. These particles were subsequently distributed into the air stream via a purpose built smoke delivery rake mounted upstream of the nozzle contraction of the wind tunnel.

DRAG MEASUREMENTS

As well as the above flow-field measurements, conventional load-cell measurements were made in order to measure the aerodynamic force contributions to the wheel. The load-cell was located inside the hub as mentioned in Figure 1.

Traditionally, a low-speed tare is subtracted from rotating wheel measurements in order to extract the aerodynamic forces. This is justified by a constant bearing drag. As the speed of the wheel increases, the rotation of the wheel induces airflow over and through the wheel. This is characterised by a velocity-squared relationship becoming apparent at the upper velocities. Figure 4 displays the wind-off rolling drag measurements for a mid-range deformation level (155mm axle height) with tyre pressure of 2.0psi (13.8kPa). This displays an always-increasing level of drag likely due to the rolling resistance of the deformable rubber. A slight velocity-squared relationship is apparent at the very top of the scale. Due to this variation, it was decided to use a full speed wind-off tare to obtain the most reliable aerodynamic forces. Due to this, the forces presented are likely to be slight underestimates of the absolute aerodynamic forces. It has been suggested that the velocity-squared relationship present at the higher velocities may be due to secondary rolling resistance effects of the tyre, however, the

previous conclusion can be justified by the pitot-static probe placed in the brake scoop, which measured a through-hub velocity to be around $2ms^{-1}$ at the top speed. However, simply subtracting a low-speed tare from such varying speed dependent mechanical forces, in order to preserve these aerodynamic effects, would have led to false trends.

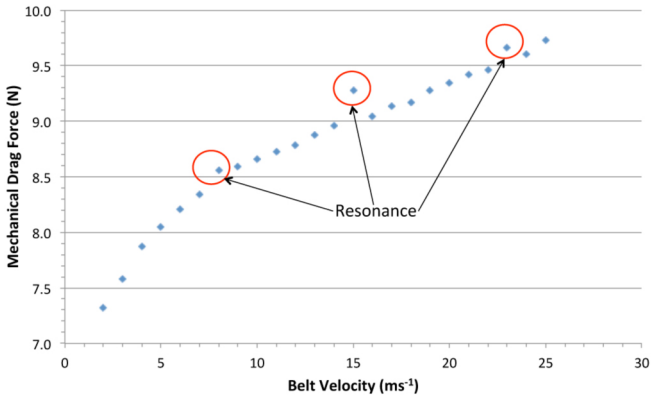

Figure 4. Velocity dependent mechanical drag force.

Figure 4 also displays evidence of resonant frequencies where small vibrations linked to the elasticity of the tyre became significant at discrete velocities. These velocities changed depending on the level of deformation (damping in the sting arm under load) and tyre pressures (hysteresis and non-uniformities in the tyre construction). It was ensured that these did not occur at the full tunnel speed and as such, some comparable axle heights for the deformation range are slightly different depending on tyre pressure (see Table 2).

RESULTS AND DISCUSSION

CONTACT PATCH MEASUREMENTS

A summary of the dimensions taken from the static contact patch measurements can be seen in Table 3 and presented with more clarity in Figure 5. As discussed in the above section, the exact contact shape was not rectangular and so a simplified elliptical model has been applied here.

Table 3. Dimensions of the contact patches.

Tyre Pressure [psi, (kPa)]	Axle Height (mm)	Length (mm)	Width (mm)
0.5, (3.4)	150	121	111
	154	106	107
	156	98	104
	159	78	105
3.0, (20.7)	150	103	100
	152	100	91
	155	94	88
	158	84	88

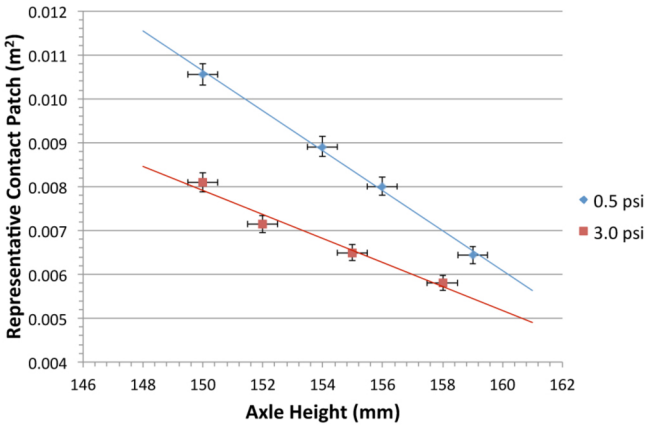

Figure 5. Representative contact patch (ellipse area based on major and minor axis measurements) against axle height (deformation level).

There is a consistent linear relationship between the size of the representative contact patch area and the level of deformation applied in terms of vertical displacement of the axle. There is also the first evidence towards discrepancies between using different tyre pressures. At 3.0psi (20.7kPa), which is relatively high for a model scale tyre, the deformation is much harder to achieve and the contact patch size is consistently lower than that of the lower tyre pressure. The delta between the contact patch size and the deformation level increases as the latter increases, which suggests that the deformation occurs in different places for different tyre pressures. For higher tyre pressures it would appear that the rate of change of contact patch is much lower than for lower pressures. It is also interesting to observe that the length of the contact patch, over this range, continues to lengthen with more deformation whereas the width appears to have reached a limit in both cases by the medium-speed cornering condition.

In both cases, the zero yaw (non-cornering condition) width of the contact patch is smaller than the width of the tyre (and indeed the non-deformed tread). The flow physics under the outboard sidewall of the tyre could therefore be expected to have a reasonable amount of low-pressure flow passing beneath it which may also strengthen the vortex features and tyre squirt observed in the flow-field.

SIDEWALL PROFILE MEASUREMENTS

The above results suggest that the deformation of the tyre changes significantly over a small range of axle heights. Figure 6 shows the sidewall profile measurement for a single tyre pressure, 3.0psi (20.7kPa), at the extreme deformation levels. These two cases are available in 3D coordinate form in Table 4 and are provided in order to allow other researches to undertake CFD experiments based upon the trends and geometries presented here.

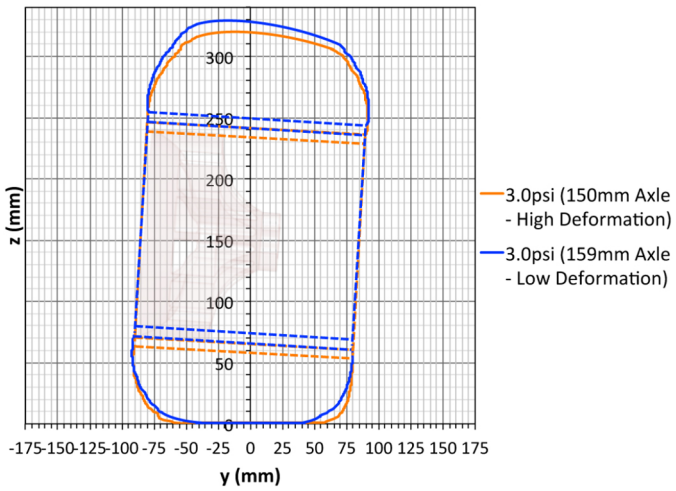

Figure 6. Comparison of the sidewall profile of the tyre at extreme deformation levels.

The figure shows how the sidewall profile is affected with varying deformation level. The most significantly affected region is the lower inboard sidewall (right hand side of figure). This shows a maximum delta of nearly 10mm showing a more abrupt and smaller radius base with more deformation. The outboard side shows the same trend. Care must be taken when studying Figure 6 as a large proportion of the delta is due to the axle height change. There is, however, an observable profile shape change too. This shows for lesser deformations, a wider upper tread width as well as describing a much less progressive curve. This method has also measured the width of the contact patch and there is good correlation with the above presentation in Table 3. A delta in tread width of the order of 15mm has been observed by both the laser profile measuring technique as well as the ink transfer method.

Figure 7 displays detail of the lower inboard sidewall of the tyre as this is the most sensitive region for varying levels of deformation. The primary purpose of this figure is to show the significant differences which take place by compromising on tyre pressure in order to minimise the vertical load required (as in Table 2). During experimental testing, an infra-red temperature gauge was used to monitor the surface temperature of the tyre after each run. The peak temperature was always measured at the inboard tread and varied by almost 20°C between maximum and minimum deformation levels. The former case, with a high tyre pressure was measured to be consistently around 80-85°C with the outboard side around 50°C. For lower tyre pressures, these were lower again, as would be predicted due to the lower vertical load used to achieve the axle height.

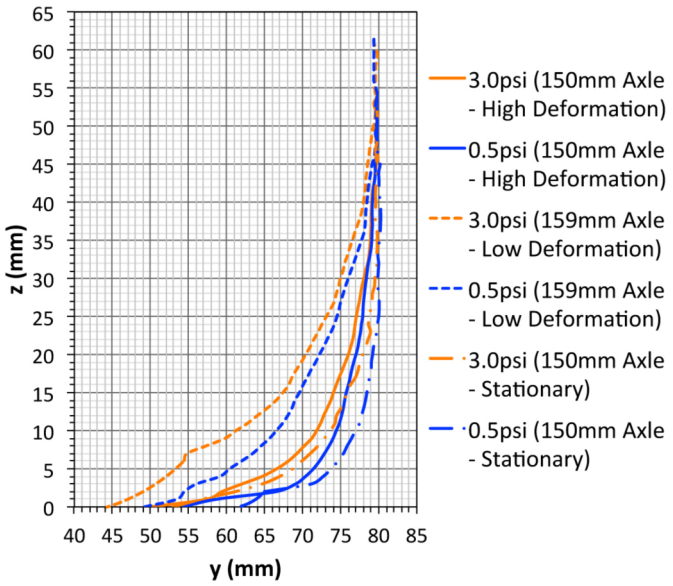

Figure 7. Comparison of the lower inboard sidewall profile of the tyre at extreme deformation levels for varying tyre pressure levels.

Initially, when stationary, it can be seen that there is a very similar contact patch region between the two different tyre pressures. However, they begin to differ after the main curvature and the lower-pressure tyre shows evidence of less deflection under load. In each case, the stationary case is more severely deformed than the high loading and in turn more so than the low loading. The low loading case shows similar deflection for both tyre pressures but there is an offset of around 4mm across the whole sidewall. Under high loading the overall tyre profile is much more square than that of the higher pressure case. The aerodynamic difference between a sharp-sided sidewall and a curved one is of high interest and will be presented in the later flow-field studies.

Figure 8 displays the profile measurement comparison between high deformation cases for the stationary and rotating cases. This shows confirmation of the 2mm average centripetal axle rise as presented earlier but also, more significantly a straighter inboard upper sidewall. This observation could be due to the lower axle height itself or a more subtle effect relating to the performance of the sidewall rubber when spinning at high speed. However, dominating both of these points is the higher overall tyre height when rotating. This will lead to larger frontal projected area and blockage of the wheel as well as differing sidewall shapes leading to altered vortices and tyre squirt in the flow-field.

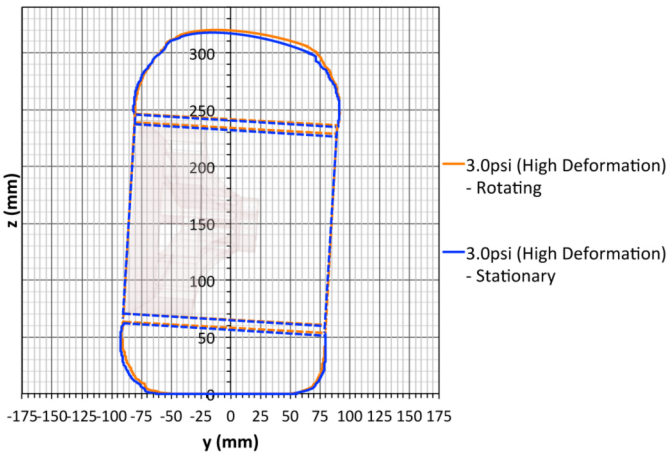

Figure 8. Comparison of sidewall profile for stationary vs. rotating cases.

FLOW-FIELD MEASUREMENTS

5-Hole Probe Crossplanes (y-z plane)

A schematic diagram of the planes interrogated has been presented in Figure 9. Figure 10 illustrates a small comparison of flow-field structures downstream of the wheel inflated to 0.5psi (3.4kPa). The left hand column shows the low deformation, high axle height cases whereas the right hand side shows the opposite extreme. Some interesting observations can be made from these wake plots. Firstly, the width of the wake is consistently wider for the lower deformation case. A contour of $Cp_0 = 0.9$ has been plotted to assist this observation. This is a contradiction to the data presented by Purvis [13], which suggested the wake widened with contact patch size. In this case, two wheel diameters (2.0D) downstream of the axle, the width of the wake has grown to 0.2D wider than the highly deformed case at a similar distance from the ground. This is a significant amount and equates to around 64mm at model scale and over 30% of the width of the tyre itself. This sensitivity is apparent and progressive through all of the cross sections when studying the stagnation pressure coefficient. Figure 11 has been included as a detailed extract of Figure 10 in order to more easily visualise the above comments.

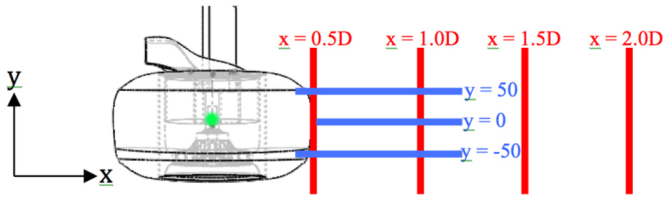

Figure 9. Schematic diagram highlighting the location of the PIV (Blue) and pressure-probe planes (Red).

The main increase in the width comes from the outboard side of the low deformation case. As discussed previously, the use of camber in an F1 tyre leads to an uneven contact patch and the full tread width does not always make contact with the road. By opening up a gap on the outboard side this encourages low-pressure flow such as that seen by Morelli [5]. This lower pressure incurs losses and encourages higher vorticity, which can be seen in the vector magnitudes.

For the low deformation case the inwash from both sides towards the centreline of the tyre appears to be split equally between the inboard and outboard side. However, this is not the case for the high deformation. Instead, a more significant flow to the outboard side of the tyre is present, particularly within one wheel-diameter to the axle. The strength of all vectors also seems to be slightly reduced, particularly in regions of high vorticity, compared to the low deformation case.

These observations are perhaps the opposite to what might be expected. It may have been assumed that for higher levels of deformation, a more aggressive sidewall to the tyre would produce a wider wake structure with higher strength vortices. The lower blockage for the low deformation case appears to be responsible for much stronger levels of downwash behind the tyre thus creating a larger counter-rotating vortex system. There is some evidence to suggest there is a larger level of jetting or tyre squirt from the low-deformation 0.5D plane (upper leftmost graph in Figure 10), particularly on the inboard side. This can be seen by the vectors pointing inboard at the ground plane and a strengthened vortex feature (around y/D = 0.8, y/D = 0.3). Despite this, both cases appear to have the same levels of total pressure loss within the wake. It is only the size of this wake that appears to differ.

There is evidence, far inboard of the tyre, of a strong counter-clockwise rotating vortex (one wheel diameter inboard of the centreline). This appears to be due to the inboard sting as illustrated in Figure 1 combined with the strong jetting from the inboard side of the wheel. In addition to the downwash in this region, the symmetrical sting in ground proximity has formed a vortex feature where the diagonal support begins. This has slightly suppressed the inboard vortex usually seen in the profiles downstream of the tyre but not significantly enough to cause it to change its character. This strengthens the argument for performing this study in isolation, as the double-wishbone suspension of an F1 car, among many other components would normally cause many vortex features, which would make isolating parameters relating to the deformable tyre almost impossible. Here we can see conclusive deltas in the size and directional behaviour of the wake in order to establish which variables are most important to recreate in full model testing.

The effect of tyre pressure on the downstream wake is small. Close to the wheel there is evidence of slightly more jetting on the inboard side but this is suppressed before 2.0D downstream and has not been presented here. Two wheel diameters downstream the flow-fields appear almost identical and this is a very important conclusion in terms of the

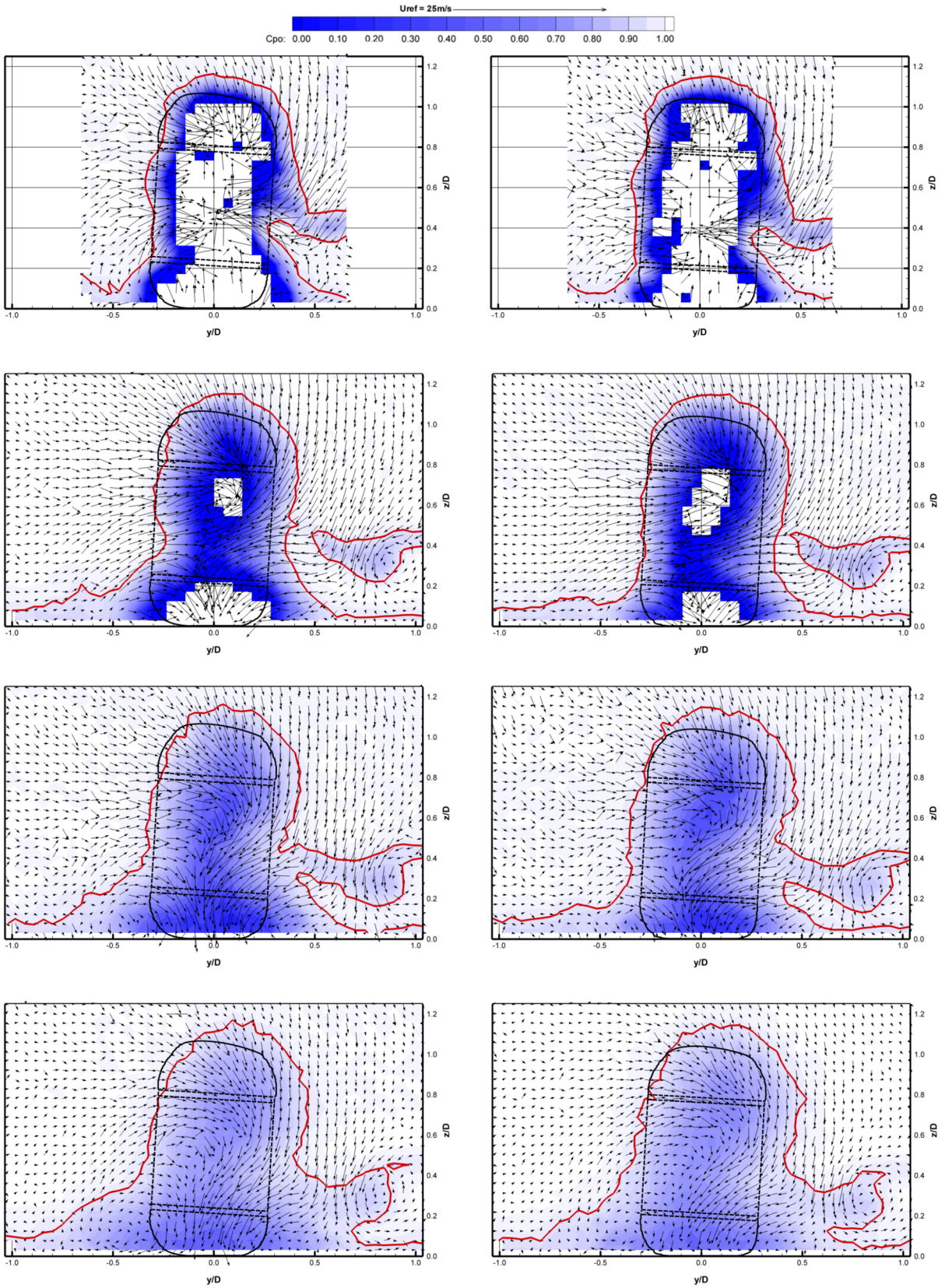

Figure 10. Comparison of the 5-hole probe measured wake data for 0.5psi inflated tyre at low (left) and high deformation (right). Rows from top to bottom at x = 0.5D, 1.0D, 1.5D and 2.0D downstream from axle respectively. Red outline - Cp0 = 0.9

practical usage of deformable tyres in a wind tunnel environment.

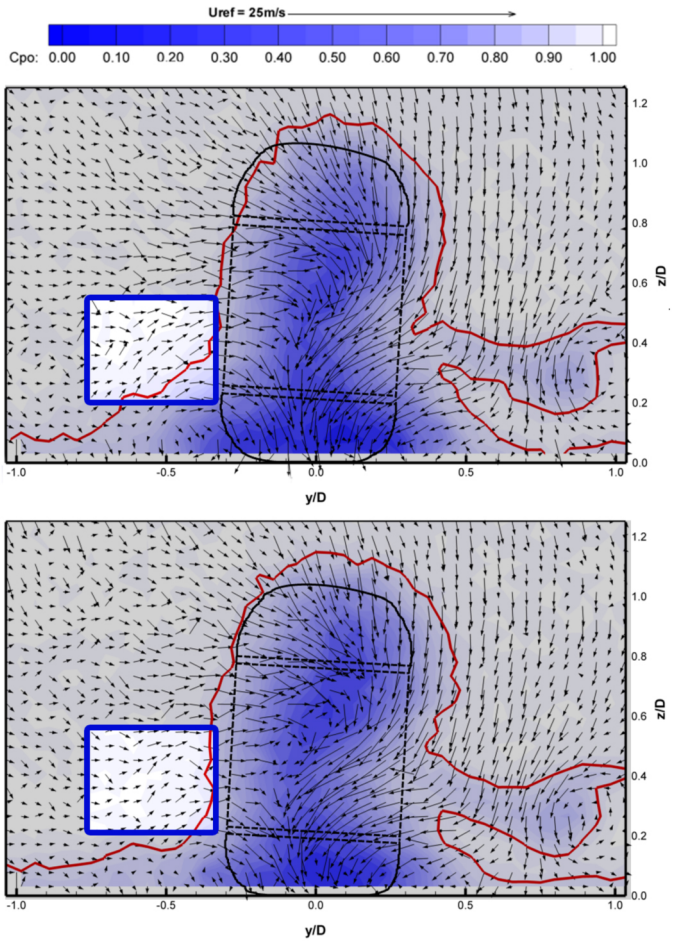

Figure 11. Extract of Fig. 10 ***(y-z plane, 1.5D downstream from axle). Upper: low deformation (high axle); Lower: high-deformation. The non-shaded region on the outboard side illustrates the change in strength of vectors as well as the overall size and form of the wake.***

PIV (x-z plane)

The PIV measurements show a similar trend to the probe measurements. From Figure 12, a comparison between centreline longitudinal planes, the wake illustrates the same increase in size and velocity, hence losses and reduction in stagnation pressure for the lower deformations. Indeed, this is the case for Figures 13 and 14, which correspond to the outboard and inboard edges of the tread respectively.

The primary observation of all of these results, is that the flow-field over the whole range drops by an order of around 10mm for the lower axle case. This is no surprise given the change in axle height and therefore overall tyre height is 9mm. Further to this, the separation point of the flow over the wheel appears to have moved forward in the high deformation case, particularly on the inboard side. This would be consistent with a larger aspect ratio, in the case of the less deformed case here, presenting larger wake and therefore increased drag as shown in Fackrell and Harvey [2]. Their surface pressure measurements using different sidewall profiles show that a more curved or less aggressive sidewall, such as that of a highly inflated tyre under any load, leads to earlier separation.

From Figure 14, the lower recirculation lobe appears to be the most sensitive region, which is perhaps not surprising given the profile measurements made earlier. In the highly deformed case the extent of this lobe ranges from 0.60D to 0.82D downstream of the axle. For a lower loading, this extends to 1.00D. This illustrates high inboard sensitivity to both tyre pressure as well as deformation level with the latter being the most significant.

For the upper lobe the sensitivity is much less prominent. Comparing tyre pressures, only evidence of earlier separation is obvious with a larger lobe resulting from the higher tyre pressure. Between deformation levels, there is a much less obvious change.

In all cases the lower deformations seem to over-speed the flow in the freestream direction as well as the recirculating lobes. This is consistent with the lower loss flow presented in Figure 10.

DRAG MEASUREMENTS

Figure 15 displays the relationship of the drag coefficient (constant reference area of 0.0535m^2) with the level of deformation. Three different tyre pressures are presented illustrating the similarity between them all at low deformations (high axle heights).

At lower axle heights, toward the high deformation end of the scale, there is an obvious discrepancy between aerodynamic drag forces. The general trend for all tyre pressures shows a decreasing drag coefficient with increasing vertical load. This is possibly due to the observation in Figure 6 where the higher deformation exhibits a slightly smaller projected frontal area than the low deformation case. The rate of change, however, is significantly different depending on the tyre pressure. This difference can only be explained by, and is consistent with, the trends in the size of the wake. For the lower deformations it was concluded that the wake structures were of higher velocity, lower stagnation pressure and covered a much larger region.

Despite the sidewall profile measurements (Figure 7) showing definite differences between the two extreme tyre pressures at low deformation levels (high axle heights), this result shows the aerodynamic drag force is relatively unaffected by this. This is perhaps surprising given the earlier separation the high-pressure tyre illustrates in the PIV measurements.

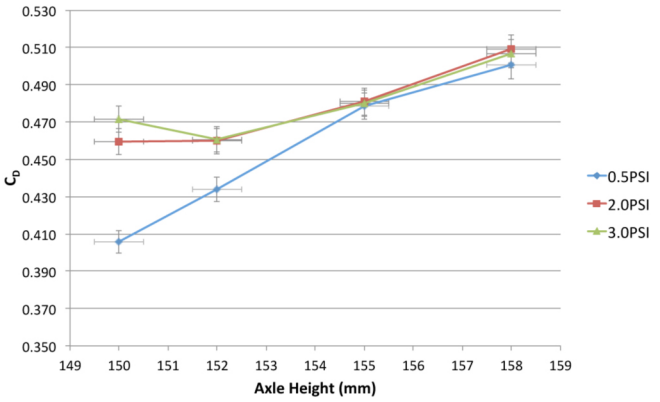

Figure 15. Aerodynamic drag measurements with constant area assumption.

All of these observations lead to a greater drag for lower deformation (higher axle height) conclusion. The more curved sidewall of the higher-pressure tyre shows more sensitivity to wake structure change than the more abrupt shape. Therefore for the two lower pressures, the drag curve is very similar. Once a certain limit is reached, the sidewall presents a curved bulge as opposed to a flat fold at the shoulder leading to the conclusions made.

CONCLUSIONS

The aerodynamic performance of the tyre is known to be of significant importance to the design of an F1 car. The results presented here have led to some important conclusions regarding the efficient and accurate representation of rotating-wheel flows.

The first observation draws from the simple rotation of the tyre. Ignoring aerodynamic effects initially, the centrifugal forces on the tyre pushing the sidewalls to a more extended and straighter profile result in an axle rise of the order of 2mm at 50% model scale. This must be taken into account when testing the tyre. Further to this, the mechanical forces at work on a deformable tyre are far more complex than that of a rigid wheel model due to the losses and hysteresis in the tyre with a higher rolling resistance. The low-speed load tare is no longer applicable due to the ever-increasing mechanical drag force all the way up the speed range. As velocity increases ($22ms^{-1}$ and beyond), there exists a velocity-squared component and evidence of induced through-hub flow, which confirms aerodynamic effects are beginning to take effect.

Manufacturer-specific tyres will deform by different amounts and in different ways, therefore careful focus has been applied to the fundamental parameters of contact patch and sidewall shape of the tyre as opposed to presenting the tyre-specific parameters such as axle height or tyre pressure used to best represent the flow-field.

The trends displayed suggest that failing to provide high enough levels of deformation (set by axle height) will lead to larger wake structures with increased drag forces. This can be as large as one fifth of a wheel diameter in width at its widest point (over a third of the tyre width). There is also less global outwash than for a more highly deformed tyre. A later inboard separation point, as observed in PIV measurements, would also infer an increased lifting load on the tyre although this has not been directly measured in this work. The overestimation of values, coupled with an incorrect flow-field as far downstream as two wheel diameters, could lead to false directions in vehicle design, particularly for the front of floor and sidepod region.

When comparing the discrepancies between tyre pressures, the sensitivity seems less significant than the level of deformation itself. Despite this, higher tyre pressures do appear to have some large changes in the local flow. This is particularly visible in the lower inboard recirculation lobe. Further downstream of the tyre the changes are minimal. Therefore it could be argued that in order to improve belt and tyre longevity in an F1 design environment (where far-field downstream wake is of primary concern), a compromise in tyre pressure is a less detrimental one to make than failing to apply enough loading to change the sidewall shape and set a correct axle height.

The contact patch area is inversely proportional to axle height, even at a notable wheel camber angle, and the rate of this changes significantly depending on the tyre inflation pressure. The reversal of the wake to contact patch trend, when compared to the limited literature, can lead to a conclusion that the flow-field is dominated by the sidewall shape and not by the contact patch. However, further work would be required in order to confirm this statement.

In conclusion, the use of deformable tyres in a wind tunnel environment is the only way to represent the correct flow-field of the F1 car on-track. Due to the number of parameters, including but not limited to contact patch size, axle height, tyre pressure, manufacturer specific construction and maintaining constant temperatures and coefficient of friction between the moving ground plane and the tyre's tread, the modelling can be as inaccurate as the usage of rigid tyres if not set up correctly. The presented experimental work has led to the conclusion that the sidewall shape is highly sensitive to vertical load and its effect on the aerodynamic performance of the wheel is significant. In order to maintain the life of test equipment, care should be made to set axle heights equivalent to those seen on-track with the lowest tyre pressure which allows a visibly curved bulge rather than a flat fold at the inboard lower edge. Thus the correct axle height and deformation level can be achieved whilst minimising vertical loading.

REFERENCES

1. Dominy, R. G., Aerodynamics of Grand Prix Cars. Proc. Instn Mech. Engrs. Part D, 206D, pp267-274, 1992.
2. Fackrell, J. E. and Harvey, J. K., The Flow Field and Pressure Distribution of an Isolated Road Wheel, Advances in Road Vehicle Aerodynamics. BHRA Fluid Engineering Conference - Paper 10, 1973.

3. Fackrell, J. E. and Harvey, J. K., The Aerodynamics of an Isolated Road Wheel. Proceedings of the Second AIAA Symposium of Aerodynamics of Sports and Competition Automobiles, Vol. 16, 1975.
4. Fackrell, J. E., The Aerodynamics of an Isolated Wheel Rotating in Contact with the Ground. PhD Thesis, University of London. 1974.
5. Morelli, A., Aerodynamic Effects on an Automobile Wheel. Technical Report Trans. 47/69, MIRA, 1969.
6. Stapleford, W. R. and Carr, G. W., Aerodynamic Characteristics of Exposed Rotating Wheels. Technical Report 1970/2, MIRA, 1970.
7. Saddlington, A. J., Knowles, R. D., Knowles, K., Laser Doppler Anemometry Measurements in the Near-Wake of an Isolated Formula One Wheel, Springer-Verlag, Exp. Fluids 42:671-681, 2007.
8. Mears, A., Dominy, R., and Sims-Williams, D., "The Air Flow About an Exposed Racing Wheel," SAE Technical Paper 2002-01-3290, 2002, doi:10.4271/2002-01-3290.
9. Mears, A., Crossland, S., and Dominy, R., "An Investigation into the Flow-Field About an Exposed Racing Wheel," SAE Technical Paper 2004-01-0446, 2004, doi:10.4271/2004-01-0446.
10. Mears, A. P., Dominy, R. G., Sims-Williams, D. B., The Flow About an Isolated Rotating Wheel - Effects of Yaw on Lift, Drag and Flow Structure, 4th MIRA Int. Vehicle Aerodynamics Conf., Warwick, UK, October 2002.
11. Mears, A. P., The Aerodynamic Characteristics of an Exposed Racing Car Wheel. PhD Thesis, University of Durham, 2004.
12. Sprot, A., Minto, J., Sims-Williams, D., and Dominy, R., "Aerodynamic Investigation on the Effect of Varying Through-Hub Flow on a Formula One Front Wheel Assembly," *SAE Int. J. of Passeng. Cars - Mech. Syst.* 4(1):929-944, 2011, doi:10.4271/2011-01-1431.
13. Purvis, A. R., The Wake Behind a Deformable Racing Tyre. MSc Thesis, Cranfield University, 2003.
14. Axerio, J., Iaccarino, G., Issakhanian, E., Lo, K. et al., "Computational and Experimental Investigation of the Flow Structure and Vortex Dynamics in the Wake of a Formula 1 Tire," SAE Technical Paper 2009-01-0775, 2009, doi:10.4271/2009-01-0775.
15. Sims-Williams, D. B., Dominy, R. G., The Design of a New Wind Tunnel for Vehicle Aerodynamics Research. 4th MIRA International Vehicle Aerodynamics Conference, Warwick, UK, October 2002.
16. Sims-Williams, D. and Dominy, R., "The Design of an Open-Jet Wind Tunnel for Model Testing," SAE Technical Paper 2002-01-3340, 2002, doi:10.4271/2002-01-3340.

CONTACT INFORMATION

Mr. Adam Sprot (a.j.sprot@durham.ac.uk)
Durham University, School of Engineering and Computing Sciences, South Road, Durham DH1 3LE. U.K.

DEFINITIONS/ABBREVIATIONS

C_D
Aerodynamic Drag Coefficient

Cp_0
Stagnation Pressure Coefficient

CFD
Computational Fluid Dynamics

D
Wheel Diameter (320mm)

DEHS
Di(2-ethylhexyl)sebacate, sebacic acid

LDA
Laser Doppler Anemometry

PIV
Particle Image Velocimetry

U
Local Velocity

Uref
Reference Velocity

APPENDIX

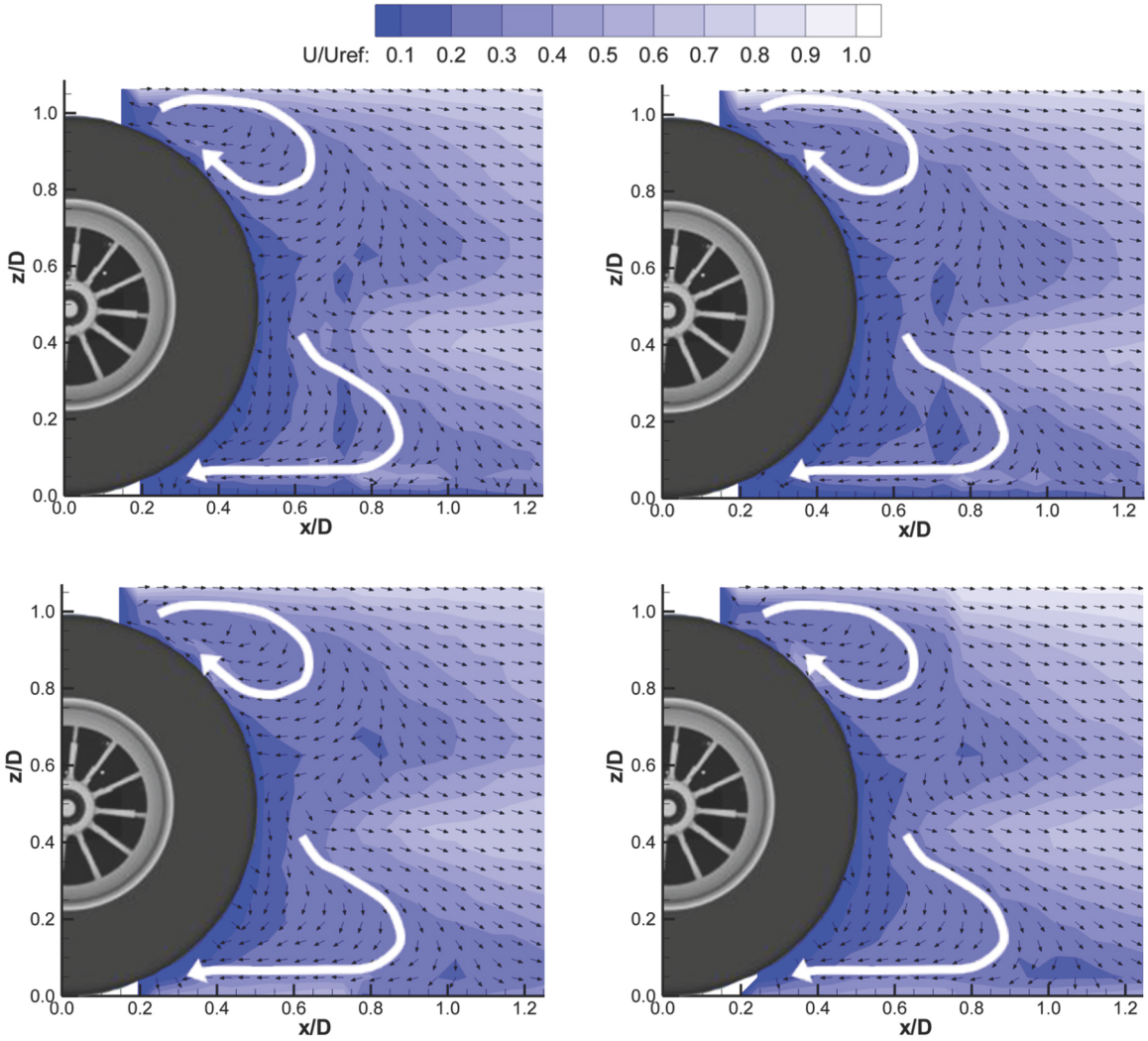

Figure 12. Centreline of tyre PIV : (Left) Low deformation; (Right) High Deformation; (Top) 0.5psi Tyre Pressure; (Bottom) 3.0psi Tyre Pressure. The flow-field of the centreline is apparently unaffected by the deformation level or tyre pressure.

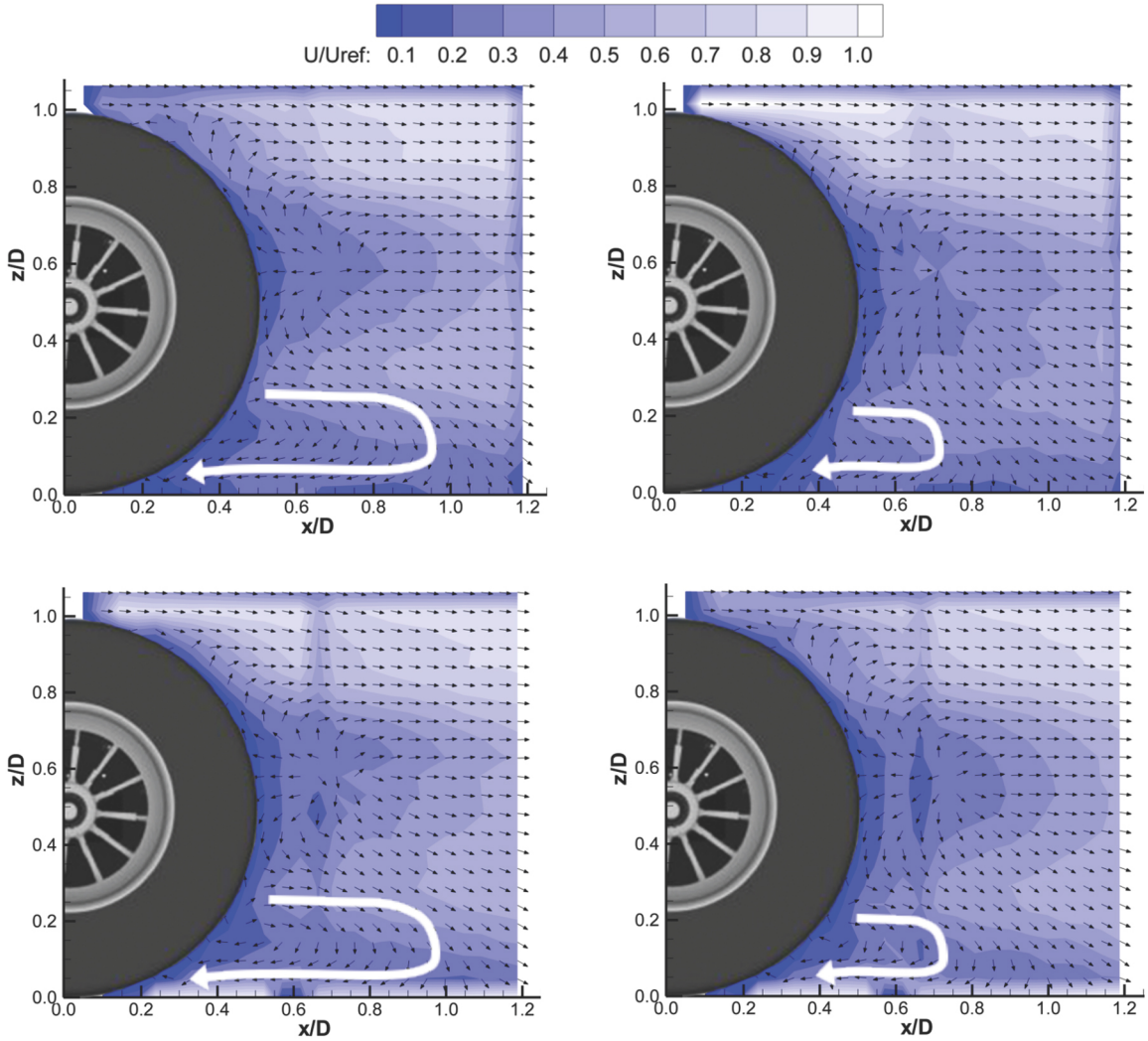

Figure 13. Outboard Tread (Y = −50mm) of tyre PIV : (Left) Low deformation; (Right) High Deformation; (Top) 0.5psi Tyre Pressure; (Bottom) 3.0psi Tyre Pressure. Low deformation leads to a larger local recirculation lobe at the outboard contact patch.

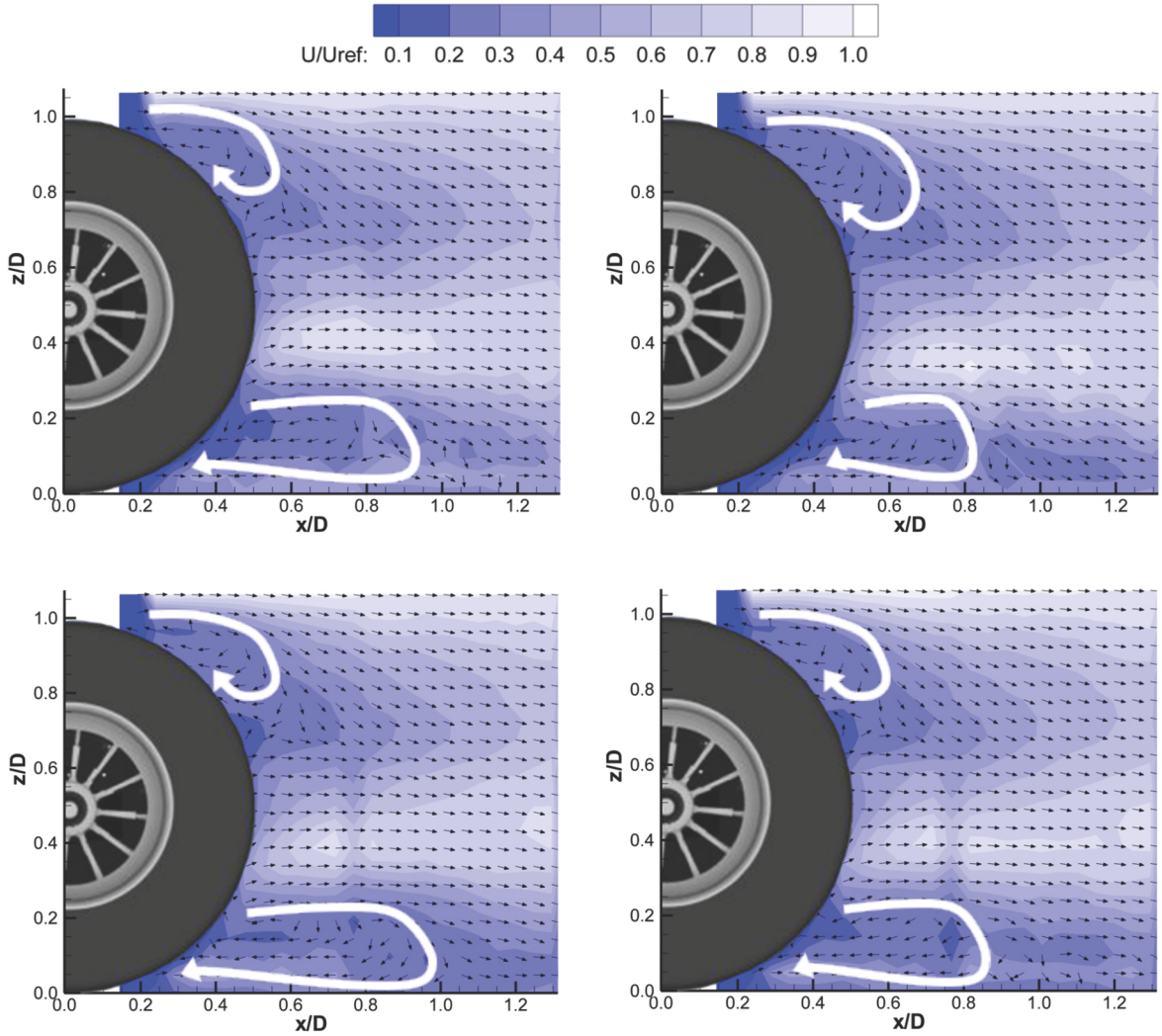

Figure 14. Inboard Tread (Y = +50mm) of tyre PIV : (Left) Low deformation; (Right) High Deformation; (Top) 0.5psi Tyre Pressure; (Bottom) 3.0psi Tyre Pressure. Upper recirculation lobe appears mostly unaffected but lower lobe exhibits the same trend as in Figure 13***.***

Table 4. Three-dimensional coordinates of 3.0psi (20.7kPa) inflation pressure at high deformation (150mm mid-axle height - model scale) and low deformation (159mm mid-axle height - model scale)

High Deformation (150mm) 3.0psi (20.7kPa)											
Lwr Inboard (x = 0)		**Upr Inboard (x = 0)**		**Upr Outboard (x = 0)**		**Lwr Outboard (x = 0)**		**Horiz Inboard (z = 150)**		**Horiz Outboard (z = 150)**	
y (mm)	**z (mm)**	**y (mm)**	**z (mm)**	**y (mm)**	**z (mm)**	**y (mm)**	**z (mm)**	**± x (mm)**	**y (mm)**	**± x (mm)**	**y (mm)**
50.00	0.00	89.97	236.61	-79.77	246.10	-50.00	0.00	88.00	84.87	88.00	-84.87
57.42	1.00	91.67	247.00	-79.73	254.00	-59.76	1.00	92.00	85.71	92.00	-84.93
59.39	2.00	91.35	259.00	-78.86	262.00	-61.49	2.00	96.00	85.74	102.00	-84.62
62.00	3.00	89.33	267.00	-77.00	270.00	-67.04	3.00	108.00	84.32	108.00	-83.93
68.10	6.00	88.56	271.00	-73.89	278.00	-69.58	4.00	116.00	82.20	114.00	-82.32
71.82	10.00	87.72	273.00	-69.45	286.00	-70.72	5.00	124.00	78.99	120.00	-80.13
75.22	18.00	85.55	277.00	-64.46	294.00	-71.55	7.00	132.00	74.80	126.00	-77.42
77.23	26.00	84.20	281.00	-58.93	300.00	-73.58	9.00	140.00	69.44	132.00	-73.88
78.04	30.00	78.92	289.00	-58.23	302.00	-80.20	15.00	148.00	63.17	138.00	-69.81
78.81	34.00	76.73	293.00	-54.56	306.00	-84.52	23.00	154.00	58.17	144.00	-65.71
78.99	38.00	76.12	295.00	-53.89	308.00	-87.95	31.00	156.00	54.52	150.00	-61.54
79.28	42.00	74.26	297.00	-51.72	310.00	-90.26	39.00	158.00	50.14	154.00	-56.34
79.87	46.00	72.53	299.00	-47.78	312.00	-90.92	47.00	160.00	43.99	156.00	-52.06
79.67	50.00	66.69	304.00	-43.06	315.00	-91.27	55.00	162.00	32.17	158.00	-45.67
79.77	53.90	62.81	306.00	-41.47	316.00	-89.97	63.39	163.00	20.64	160.00	-30.96
Low Deformation (159mm) 3.0psi (20.7kPa)											
Lwr Inboard (x = 0)		**Upr Inboard (x = 0)**		**Upr Outboard (x = 0)**		**Lwr Outboard (x = 0)**		**Horiz Inboard (z = 159)**		**Horiz Outboard (z = 159)**	
y (mm)	**z (mm)**	**y (mm)**	**z (mm)**	**y (mm)**	**z (mm)**	**y (mm)**	**z (mm)**	**± x (mm)**	**y (mm)**	**± x (mm)**	**y (mm)**
44.00	0.00	90.34	244.22	-79.35	254.45	-44.00	0.00	88	84.86	88.00	-84.87
54.45	6.00	91.55	246.00	-80.28	258.00	-62.11	7.00	96.00	84.88	92.00	-84.55
57.30	8.00	92.08	250.00	-79.74	266.00	-66.00	8.00	104.00	83.98	98.00	-84.54
61.21	10.00	92.10	264.00	-78.62	274.00	-68.81	9.00	112.00	82.11	104.00	-84.05
64.05	12.00	91.32	268.00	-77.73	278.00	-72.21	12.00	120.00	79.43	110.00	-83.20
66.52	14.00	90.75	272.00	-76.17	282.00	-76.16	16.00	124.00	77.66	116.00	-81.33
69.16	18.00	89.64	276.00	-73.23	290.00	-81.63	24.00	132.00	73.21	122.00	-78.90
71.47	22.00	87.17	282.00	-70.62	294.00	-84.21	28.00	136.00	70.76	134.00	-72.16
73.67	26.00	85.91	286.00	-65.93	302.00	-86.39	32.00	144.00	65.31	140.00	-67.88
74.94	30.00	84.97	288.00	-62.66	306.00	-89.23	40.00	148.00	61.28	146.00	-62.88
77.55	38.00	81.85	292.00	-59.72	310.00	-91.25	48.00	152.00	58.69	150.00	-60.98
78.68	46.00	79.83	296.00	-56.60	314.00	-91.63	52.00	154.00	54.96	152.00	-58.79
79.49	51.00	77.12	301.00	-53.69	318.00	-92.04	60.00	156.00	50.95	154.00	-55.62
79.49	55.00	74.16	303.00	-49.39	322.00	-91.65	64.00	158.00	45.68	156.00	-51.10
79.80	59.00	72.85	307.00	-46.03	324.00	-90.92	70.00	160.00	36.38	158.00	-43.33
79.35	61.55	70.09	309.00	-41.99	326.00	-90.34	71.78	162.00	18.12	160.00	-24.08